Available online at https://link.springer.com/journal/42241
http://www.jhydrodynamics.com
Journal of Hydrodynamics, 2021, 33(6): 1230-1241
https://doi.org/10.1007/s42241-022-0108-2

Pressure fluctuation characteristics in the pressurization unit of a multiphase pump*

Guang-tai Shi[1, 3], Zong-ku Liu[2, 4], Ye-xiang Xiao[3], Xue-lin Tang[2, 4], Xiao-bing Liu[1]
1. *Key Laboratory of Fluid and Power Machinery, Ministry of Education, Xihua University, Chengdu 610039, China*
2. *College of Water Resources and Civil Engineering, China Agricultural University, Beijing 100083, China*
3. *State Key Laboratory of Hydroscience and Engineering and Department of Energy and Power Engineering, Tsinghua University, Beijing 100084, China*
4. *Beijing Engineering Research Centre of Safety and Energy Saving Technology for Water Supply Network System, China Agricultural University, Beijing 100083, China*

(Received March 13, 2021, Revised April 24, 2021, Accepted May 17, 2021, Published online January 7, 2022)

Abstract: The tip clearance induces the tip leakage vortex (TLV), which has a great impact on the pressure fluctuation characteristics of the multiphase pump. To investigate the effect of the tip clearance on the pressure fluctuations, based on the Reynolds time-averaged Navier-Stokes equation and the shear stress transfer (SST) k-ω turbulence model, the three-dimensional turbulent flow in the pump is numerically simulated for different tip clearances in the water and gas-liquid two-phase cases by using the ANSYS CFX software and the results are verified with experimental data. It is shown the greater pressure fluctuation intensity corresponds with the TLV both in the water and gas-liquid two-phase cases. In the meantime, the location of the maximum pressure fluctuation intensity is related to the tip clearance size. In addition, for different tip clearances, the pressure fluctuation intensity with the rotor and stator interaction (RSI) is relatively larger. The difference is that when $R_{tc}=1.5$ mm, the pressure fluctuation intensity near the impeller middle point is also relatively larger. On the whole, the pressure fluctuation intensity in the gas-liquid two-phase case is larger than that in the water case. Furthermore, the gas causes the frequency of the high-amplitude pressure fluctuation in the impeller and the diffuser to be shifted from $7f_n$ (f_n denotes impeller rotational frequency) and $3f_n$ to the low-frequency region, respectively. The pressure fluctuations at the blade-passing frequency (BPF) and the multiple BPFs gradually disappear. Meanwhile, the amplitude at the dominant frequency in the gas-liquid two-phase case is at least one order of magnitude smaller than that in the water case, and the peak-to-peak value of the pressure fluctuation is also much smaller.

Key words: Multiphase pump, gas void faction, pressure fluctuation intensity, tip leakage vortex (TLV), numerical simulation

Introduction

As the core of the multiphase transportation technology, the multiphase pump is widely used in the deep-sea oil and gas development[1-3]. According to its working principle, the multiphase pump can be divided into two types: the rotodynamic pump and the positive displacement pump[4-6]. Compared with the positive displacement multiphase pump, the rotodynamic multiphase pump has the advantages of small volume, large flow, insensitivity to solid particles, and easy to use and maintain. The rotodynamic multiphase pump (as simply called the multiphase pump) is composed of the rotational impeller and the stationary diffuser. In the meantime, to avoid friction, a certain gap is left between the impeller blade tip and the shroud[7-9]. During the operation of the pump, the rotor and stator interaction (RSI) between the impeller and the diffuser causes periodic pressure fluctuations and leads to vibration and noise. Meanwhile, due to the existence of the tip clearance, the tip leakage flow (TLF) is formed under the action of the pressure difference between the pressure side (PS) and the suction side (SS). The tip leakage vortex (TLV) is developed, which further aggravates the stability in operation[10-11].

Studies at home and abroad were widely carried

* Projects supported by the National Key Research and Development Program of China (Grant No. 2018YFB0905200)
Biography: Guang-tai Shi (1985-), Male, Ph. D., Associate Professor
Corresponding author: Guang-tai Shi,
E-mail: shiguangtai_1985@126.com

out for the characteristics of the TLV and the pressure fluctuation in the pump. For the multiphase pumps, Xu et al.[12] experimentally investigated the characteristics of the pressure fluctuation, and it was found that the dominant frequency of the pressure fluctuation in the water and gas-liquid two-phase cases is the blade passing frequency (BPF). At the impeller downstream, the pressure fluctuation is significantly weakened. Shi et al.[13-14] applied the ANSYS CFX software to study the characteristics of the TLV in a multiphase pump. It was suggested that the inlet gas void fraction (IGVF) has a significant impact on the TLV structure and trajectory. Meanwhile, in the water case, the TLV is distributed in a wave style in the flow passage. Based on the Euler-Euler two-fluid model, Zhang et al.[15] employed ANSYS CFX software to explore the pressure fluctuation characteristics in a multiphase pump with different IGVFs. It was indicated that the RSI is still the main driving force of the pressure fluctuation in the gas-liquid two-phase case, and the variation trends of the pressure fluctuation along the streamwise direction are similar for different IGVFs. Zhang et al.[16] used the computational fluid dynamics (CFD) method to study the transient flow characteristics in a multiphase pump with different tip clearances, and it was pointed out that the dominant frequency and the maximum amplitude of the pressure fluctuations increase with the increase of the tip clearance. For the axial flow pump, Feng et al.[17] studied the effect of the tip clearance on the pressure fluctuation in an axial flow pump, and it was concluded that as the tip clearance increases, the pressure fluctuation in the entire impeller domain is increased, however, not in the diffuser domain. Shen et al.[18] adopted the ANSYS Fluent software to study the TLF and TLV characteristics by using the finite volume method (FVM) and the semi-implicit method for the pressure linked equations with the consistent (SIMPLEC) algorithm. It was demonstrated that as the tip clearance is increased, the TLV moves inward in the radial direction. At the same time, the tip separation vortex (TSV) moves also closer to the blade tip surface. For the mixed flow pump, Liu et al.[19] used the ANSYS CFX software to study the TLV and pressure fluctuation characteristics in a mixed flow pump on the basis of the re-normalization group (RNG) k-ε turbulence model. Simulation results indicate that when the tip clearance is increased from 0 mm to 1.0 mm, the maximum amplitude of the pressure fluctuation in the impeller is increased sharply. Hao et al.[20] employed the CFD method to study the effect of the symmetrical and asymmetric tip clearances on the energy characteristics of a mixed flow pump based on the Reynolds time-averaged Navier-Stokes equations (RANS). It was shown that the asymmetric tip clearance induces uneven TLFs, and also leads to different power capabilities for different blades. Zhang et al.[21] carried out numerical simulations to investigate the characteristics of the pressure fluctuation in a mixed-flow pump with different IGVFs. Results show that the pressure fluctuation is increased only when the IGVFs approach to a certain level. For the centrifugal pump, Wang et al.[22] used the ANSYS CFX software to study the TLV characteristics in a semi-open centrifugal pump based on the SST k-ω turbulence model and the three-dimensional RANS. It was indicated that the TLV at the leading edge (LE) of the blade gradually moves to the SS, and the TLV at the tip of the blade middle is gradually extended to the adjacent blade PS. Similarly, Ayad et al.[23] employed the CFD method to study the effect of the semi-open impeller side clearance on the centrifugal pump performance. The results suggested that as the side clearance is increased, the vortex caused by the secondary flow would hinder the flow in the impeller core region, to reduce the pump pressurization performance. Zheng et al.[24] adopted the ANSYS Fluent software to simulate the three-dimensional flow pattern in the centrifugal pump and analyzed the pressure fluctuation characteristics, based on the three-dimensional incompressible RANS equation. It was shown that the pressure fluctuation in the tip clearance is affected by the BPF, and the amplitude of the pressure fluctuation at the dominant frequency is gradually increased in the place close to the impeller outlet. The vortex cavitating flow at the blade leading edge of the inducer in a high-speed centrifugal pump was investigated by using experimental and numerical methods, and the related studies were extensively reviewed[25-26]. In addition, other parts of the turbomachinery were also extensively studied, such as the fans[27], and the compressors[28-29], with many valuable results.

As the above analyses show, the characteristics of the TLV and the pressure fluctuation in the turbomachinery were extensively investigated. However, in general, most studies were based on the analyses of single-phase media, few on those of the two-phase or even multi-phase media. For multiphase pumps, the gas-liquid two-phase flow is an essential research topic. In the meantime, the gas and liquid phases appear alternately in the deep-sea environment operations. The tip clearance changes due to the bearing deformation and the blade wear. Therefore, it is necessary to analyze the pressure fluctuation characteristics of multiphase pumps with varying tip clearances in the water and gas-liquid two-phase cases, for better understanding the effect of the tip clearance on the pressure fluctuation.

1. Research model

The basic parameters of the multiphase pump studied in the present paper are as follows: the design flow rate $Q = 100\ \mathrm{m}^3/\mathrm{h}$, the design rotational speed $n = 3\,000$ rpm, and the number of the impeller and diffuser blades, which are 3, 7, respectively. The tip clearances $R_{tc} = 0.5$ mm, 1.0 mm and 1.5 mm, which are 0.3%, 0.6% and 0.9% of the impeller diameter, respectively. The model of the impeller and the diffuser and the meridian plane parameters are shown in Figs. 1, 2, respectively. In Fig. 2, r represents the radial direction of the impeller and the diffuser. In the meantime, Z represents the rotation axis of the impeller. In addition, to ensure the flow to be fully developed in the simulation, the impeller inlet and the diffuser outlet are appropriately extended.

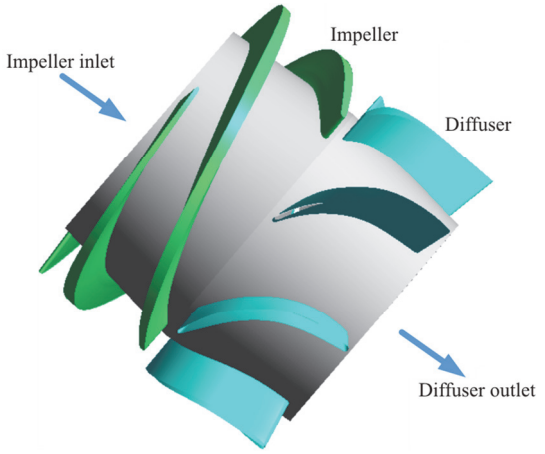

Fig. 1 (Color online) Model of the impeller and the diffuser

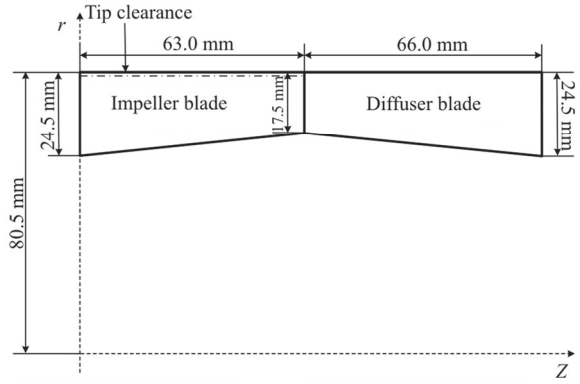

Fig. 2 Meridian plane parameters of the impeller and the diffuser

2. Numerical methods and settings

2.1 *Mesh arrangement*

To guarantee the accuracy of the simulation, the entire computational domain, including the inlet pipe, the impeller, the diffuser and the outlet pipe, is discretized by a high-quality structured mesh. The mesh quality of the impeller and the diffuser, the core component of the multiphase pump, has a direct effect on the accuracy of the simulation results. To control the boundary layer distribution near the blade, the O-type topology is employed. In the meantime, to accurately capture the detailed characteristics of the flow in the blade tip clearance, the mesh in the tip clearance is locally refined. The specific mesh is shown in Fig. 3.

2.2 *Mesh and time step independence verification*

2.2.1 Mesh independence verification

The mesh number is an important factor that determines the accuracy of the numerical simulations. To obtain the optimum mesh number for the numerical simulations, the mesh independence verification is conducted. In the first place, five sets of computational meshes with the mesh number of 2 490 070-4 726 647 are generated and named the meshes 1-5. Then, the numerical simulations are carried out with these meshes. Finally, the head/head 1 and the efficiency/efficiency 1 under different meshes (the head 1 and the efficiency 1 denote the head and the efficiency of the mesh 1) are listed in Table 1. It is shown that the mesh number has only a slight effect on the numerical results in those simulations. In a balance of the calculation cost and the accuracy, the mesh 4 is selected as the final mesh in the present work.

2.2.2 Time step independence verification

The time steps selected in the transient numerical simulation are 5.56×10^{-5} s, 1.11×10^{-4} s, and 1.67×10^{-4} s, which corresponds to the impeller rotation angle of 1°, 2° and 3°, to make the time step independent verification. Figure 4 presents the histories of the pressure fluctuation on the blade tip PS at the impeller outlet (IPS) and the diffuser inlet (DPS). As illustrated in Fig. 4, the variation trends of the pressure fluctuation are basically the same with different time steps. With consideration of the time and the accuracy, the final time step is selected as 1.11×10^{-4} s.

2.3 *Boundary conditions and settings*

In this paper, the ANSYS CFX is employed to simulate the three-dimensional transient multiphase flow in the pump with different tip clearances. To better simulate the flow field with the reverse pressure gradient and accurately predict the TLV flow pattern, the SST k-ω turbulence model is adopted. In the meantime, the Euler-Euler two-fluid model is selected for the simulation of the gas-liquid two phase flow. In

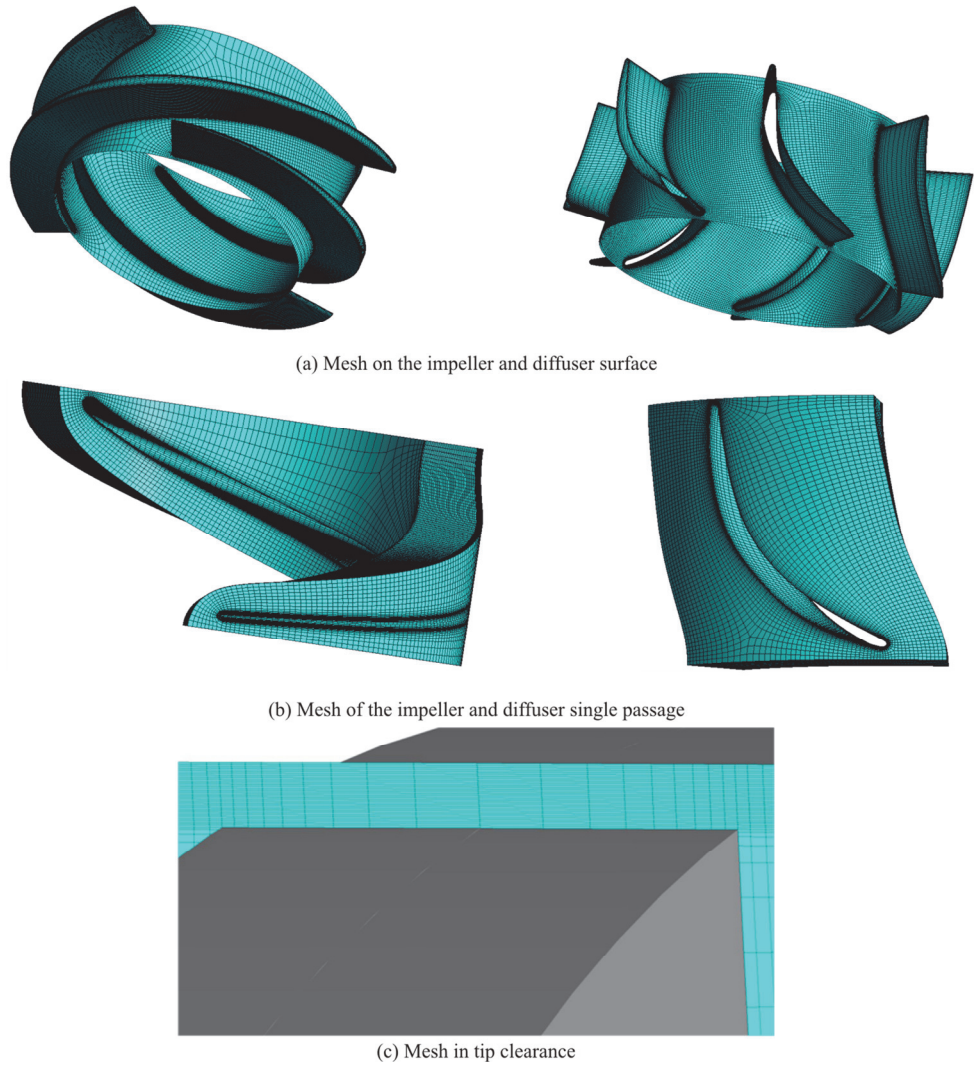

(a) Mesh on the impeller and diffuser surface

(b) Mesh of the impeller and diffuser single passage

(c) Mesh in tip clearance

Fig. 3 (Color online) Meshes of the impeller and the diffuser

Table 1 Mesh independence verification

Item	Mesh 1	Mesh 2	Mesh 3	Mesh 4	Mesh 5
Mesh number	2 490 070	2 921 104	3 251 592	3 676 610	4 726 647
Head/head1	1	1.0215	1.0179	1.0183	1.0306
Efficiency/efficiency1	1	1.0337	1.0349	1.0373	1.0542

the simulation, the boundary conditions are set as follows: the inlet boundary is set as the velocity boundary and the outlet is set as the static pressure boundary. The rotational speed, the wall boundary and the convergence residual are set as 3 000 rpm, the no-slip wall, and 10^{-5}, respectively. The interfaces of the rotational and stationary components are set as the "frozen rotor", the "transient rotor stator" in the steady and transient simulations, respectively. The steady simulation results are used as the initial value for the transient simulation, in the meantime, the transient simulation is conducted for 16 impeller revolutions and the analysis is performed based on the results of the last 6 revolutions.

2.4 *Numerical verification*

Figure 5 is a multiphase pump test rig, mainly composed of the multiphase pump, the motor, the gas-liquid mixing tank, the lubrication system, the cooling system, the control system, the water supply system, the gas supply system, the pipelines and the valves. In the experiment, the water flows from the water tank, driven by the feed pump. Meanwhile, the gas flows from the air compressor, driven by an air

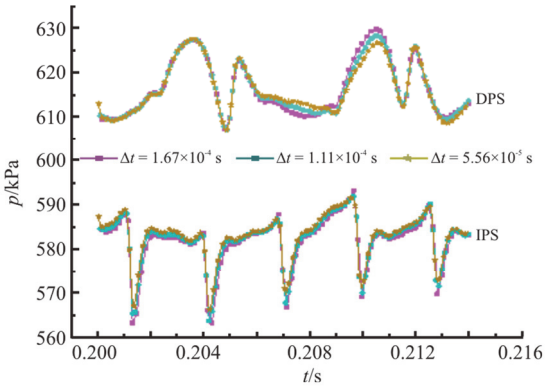

Fig. 4 (Color online) Time step independence verification

compressor. After the gas and the water are uniformly mixed in the mixing tank, they enter the multiphase pump and then return to the water tank. The camera (RDT16-4G) speed is 500 fps, and the resolution is 1 280×1 024 pixels. With a reduced resolution, the maximum speed can be 16 000 fps. The photography system has a memory of 4 GB, which stores more than 3 000 high-resolution images. In the meantime, a fully transparent plexiglass impeller shroud is used in the high-speed photography experiment, supplementing by a fill light, to capture the tip flow field more accurately.

To verify the reliability of the numerical method, the flow pattern captured by the high-speed photography is compared with the CFD results, as shown in Fig. 6. The comparison of the flow pattern near the blade tip in the experiment shows a good agreement with the CFD results, especially in the water case, which demonstrates that the numerical method is reliable.

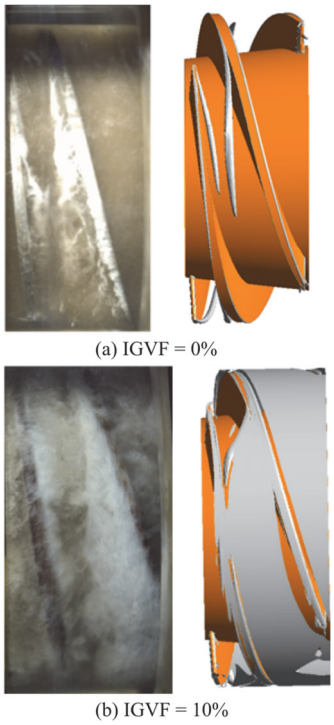

Fig. 6 (Color online) Experimental and CFD flow patterns

3. Results and discussions

3.1 *Pressure fluctuation parameter definition*

To quantitatively analyze the variations of the pressure fluctuation in the multiphase pump, the pressure fluctuation intensity and the pressure coefficient are specially defined, as follows:

$$\overline{p} = \frac{1}{N}\sum_{i=1}^{N} p_i \tag{1}$$

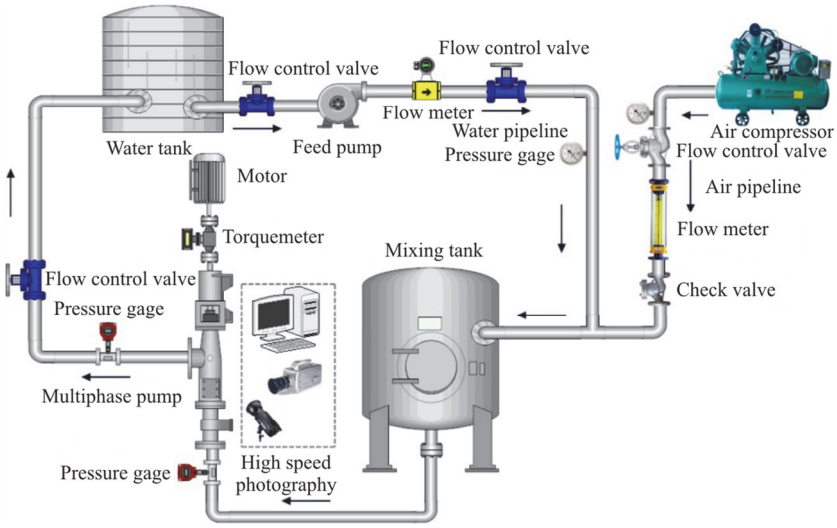

Fig. 5 (Color online) Multiphase pump test rig

$$\overline{p'} = \sqrt{\frac{1}{N}\sum_{i=1}^{N}(p_i - \overline{p})^2} \tag{2}$$

where N denotes the number of the sample points in a period, p_i denotes the pressure for each time step and $\overline{p}$ denotes the arithmetic average value in the period. To make the comparison and the analysis easy, it is nondimensionalized as follows:

$$I_{pf} = \frac{\overline{p'}}{1/2\rho U_{\text{tip}}^2} \tag{3}$$

$$C_p = \frac{p_i - \overline{p}}{1/2\rho U_{\text{tip}}^2} \tag{4}$$

where U_{tip} denotes the tip circumferential velocity with the tip clearance of $R_{tc} = 1.0$ mm, the value is 24.96 m/s and ρ denotes the water density.

3.2 *Pressure fluctuation intensity in the pressurization unit*

To investigate the effect of the tip clearance on the pressure fluctuation intensity, the pressure fluctuation characteristics in the gas accumulation region (near the tip clearance of the impeller, and the hubs of the impeller and the diffuser) are emphatically analyzed. The pressure fluctuation intensities near the shroud and the hub are presented in Figs. 7, 8, respectively. From Fig. 7, it is seen that when the tip clearance R_{tc} is equal to 0.5 mm, the maximum pressure fluctuation in the pump approaches the largest in intensity, especially, near the impeller blade LE and the diffuser inlet. At the same time, the pressure fluctuation intensity at the impeller inlet in the water case is larger than that in the gas-liquid two-phase case. When the tip clearances R_{tc} are equal to 1.0 mm, 1.5 mm, the pressure fluctuation near the impeller blade tip assumes a stripe-shape both in the water and gas-liquid two-phase cases. Meanwhile, the presence of the gas increases the pressure fluctuation intensity in the impeller inlet passage when the tip clearance R_{tc} is equal to 1.5 mm. As presented in Fig. 9, the pressure fluctuation intensities in the TLV region with different tip clearances are larger. Furthermore, in the water and gas-liquid two- phase cases, the pressure fluctuation intensities at the diffuser outlet decrease with the increase of the tip clearances. As demonstrated in Fig. 8, the location and the maximum pressure fluctuation intensity at the hubs of the impeller and the diffuser are different due to the different tip clearances. When the tip clearance R_{tc} is equal to 0.5 mm, the pressure fluctuation intensity at the rotor stator interface is the largest. The presence of the gas increases the pressure fluctuation intensity at the impeller outlet, however, it has a significant inhibition effect on the pressure intensity at the impeller inlet. When the tip clearances R_{tc} are equal to 1.0 mm, 1.5 mm, the maximum pressure fluctuation intensity is mainly concentrated near the blade PS at the impeller inlet and the rotor-stator interface. As the tip clearance increases from 1.0 mm to 1.5 mm, the maximum pressure fluctuation intensity region near the blade PS at the impeller inlet expands in the water and gas-liquid two-phase cases. Simultaneously, at the same tip clearance, the pressure fluctuation intensity near the blade PS at the impeller inlet in the gas-liquid two-phase case increases significantly. Through Figs. 7, 8, when the tip clearances R_{tc} are equal to 0.5 mm, 1.0 mm and 1.5 mm, the pressure fluctuation intensities are concentrated on the rotor stator interface, the

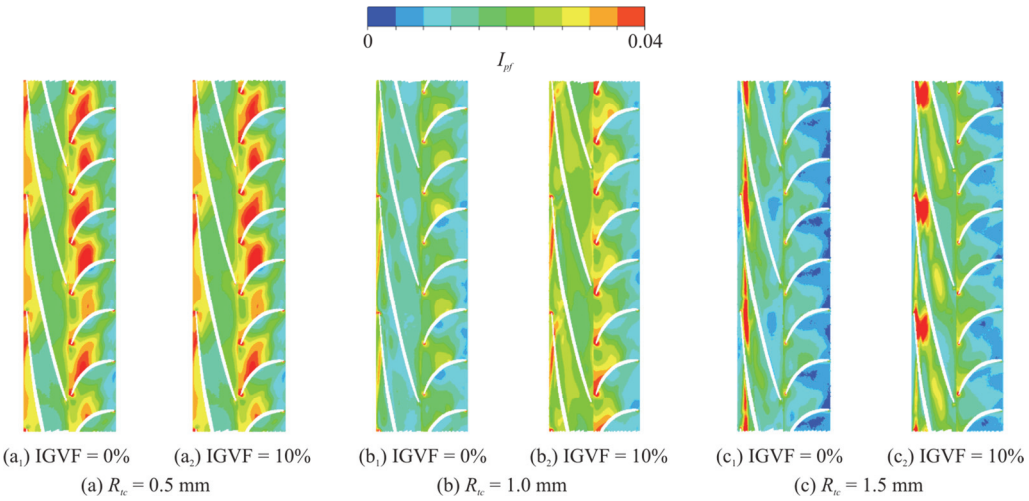

Fig. 7 (Color online) Pressure fluctuation intensity near blade tip

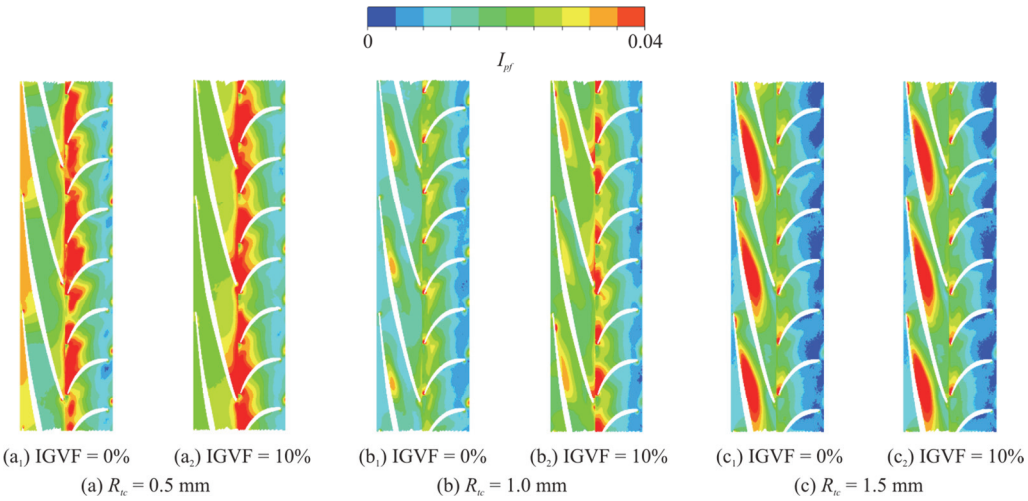

Fig. 8 (Color online) Pressure fluctuation intensity near the hub

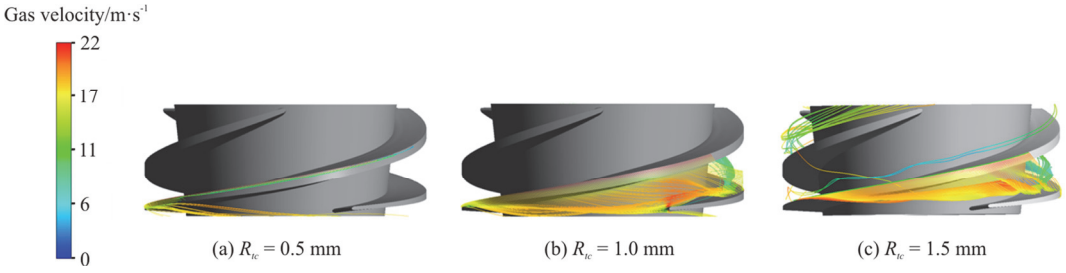

Fig. 9 (Color online) Gas streamlines near the blade tip

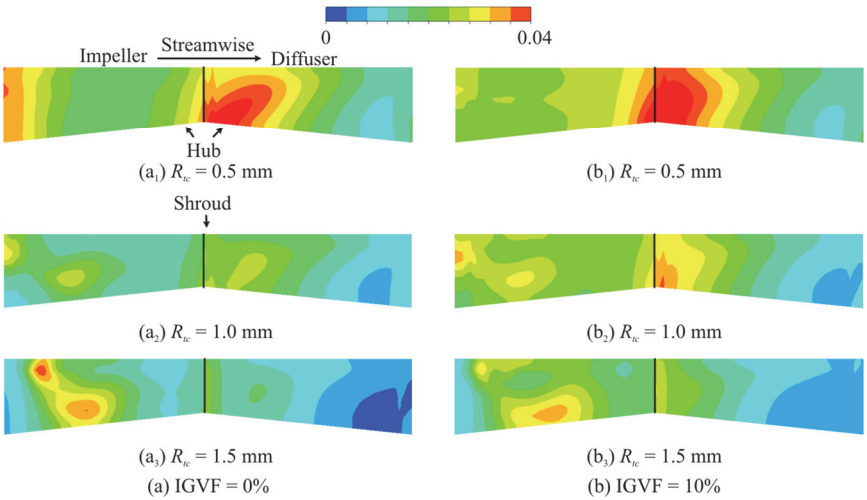

Fig. 10 (Color online) Pressure fluctuation intensity on the meridian plane of the pressurization unit

rotor stator interface and the impeller, and the impeller, respectively. In the meantime, when the tip clearance R_{tc} is equal to 1.0 mm, the maximum pressure fluctuation intensity in the impeller and the diffuser is the smallest.

Figure 10 shows the pressure fluctuation intensity in the meridian plane of the pressurization unit for different tip clearances in the water and gas-liquid two-phase cases. In Fig. 10, with the increase of the tip clearance, both in the water case and the gas-liquid two-phase case, the pressure fluctuation intensity near the rotor stator interface presents a downtrend. Meanwhile, the pressure fluctuation intensity near the hub at the diffuser outlet also gradually decreases, and the range of the minimum pressure fluctuation intensity is gradually expanded.

To quantitatively analyze the pressure fluctuation intensity along the flow direction in the pressurization unit, Fig. 11 presents the pressure fluctuation intensity along the flow direction with different tip clearances in the water and gas-liquid two-phase cases. To conveniently describe the locations along the flow direction, they are defined as follows. Along the flow direction, the impeller inlet, the rotor stator interface, and the diffuser outlet are given the values 0, 1 and 2, respectively. As illustrated in Fig. 11, for different tip clearances, the pressure fluctuation intensities near the rotor stator interface are larger, and in the gas-liquid two-phase case, the pressure fluctuation intensities of large values at the locations along the flow direction are greater than those in the water case. At the same time, the pressure fluctuation intensities from the position 1.25 in the flow direction to the diffuser outlet are almost the same both in the water and gas-liquid two-phase cases. Moreover, for different tip clearances, the pressure fluctuation intensity trends along the flow direction in the water and gas-liquid two-phase cases are different. When the tip clearance R_{tc} is equal to 0.5 mm, the pressure fluctuation intensity in the region 0.50-1.25 in the flow direction in the gas-liquid two-phase case is larger than that in the water case. However, the pressure fluctuation intensities at other locations in the water case are equal to or larger than those in the gas-liquid two-phase case. When the tip clearance R_{tc} is equal to 1.0 mm, except at the diffuser outlet, the pressure fluctuation intensity from the impeller inlet to the diffuser outlet in the gas-liquid two-phase case is equal to or larger than that in the water case. When the tip clearance R_{tc} is equal to 1.5 mm, the pressure fluctuation intensity at the flow direction of 0-0.25 is basically the same in the water and gas-liquid two-phase cases. Along the positions 0.25-0.50 in the flow direction, the pressure fluctuation intensity in the water case is larger than that in the gas-liquid two-phase case. From the position 0.5 in the flow direction to the diffuser outlet, the pressure fluctuation intensity in the gas-liquid two-phase case is larger than that in the water case. In the meantime, in the water and gas-liquid two-phase cases, the pressure fluctuation intensity near the positions 0.5, 1.0 in the flow direction is relatively larger than that at other locations. In short, although the pressure fluctuation intensities for different tip clearances show different trends, the pressure fluctuation intensities in the gas-liquid two-phase case are generally larger than those in the water case.

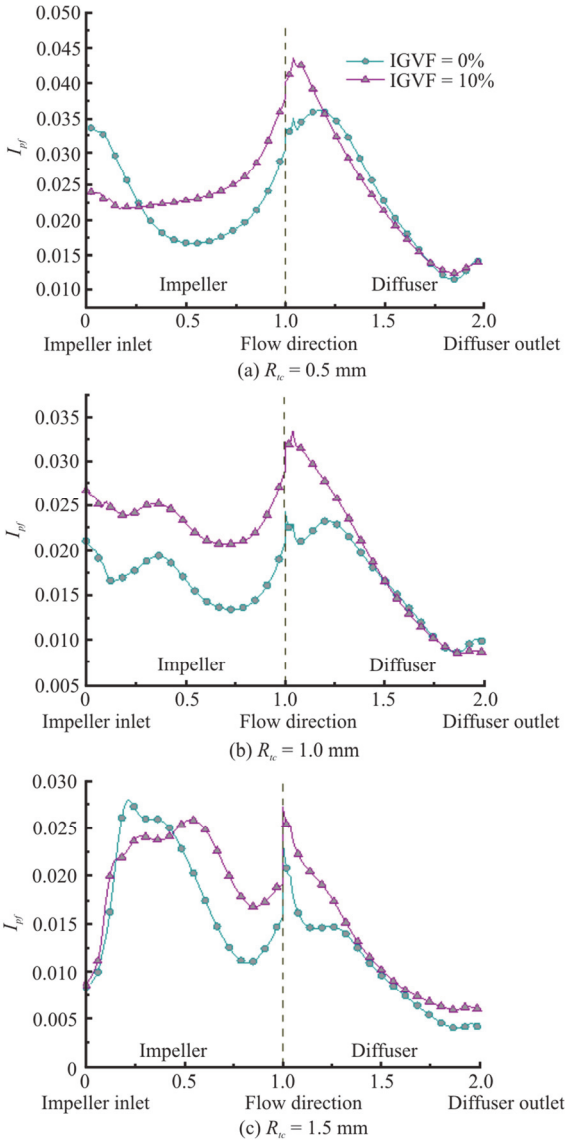

Fig. 11 (Color online) Pressure fluctuation intensity in the flow direction in impeller and diffuser

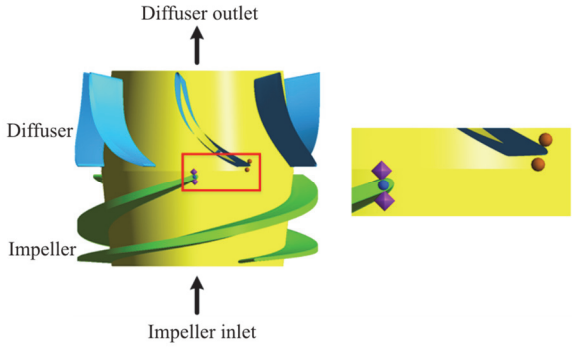

Fig. 12 (Color online) Survey points

3.3 *Spectral characteristics near impeller and diffuser blade tip*

To reveal the effects of the IGVF and the tip clearances on the pressure fluctuation spectral characteristics of the pump, the survey points are arranged

near the PS, the tip clearance and the SS at the impeller outlet, which are named as IPS, TC and ISS, respectively. Meanwhile, the survey points are also arranged near the PS and the SS at the blade tip at the diffuser inlet, which are named as DPS, DSS, respectively. The details of the survey points are shown in Fig. 12.

Figure 13 displays the spectral characteristics of the pressure fluctuation at the survey points for different IGVFs and tip clearances. The rotational speed of the multiphase pump is 3 000 rpm, thus, the impeller rotational frequency $f_n = n/60 = 3000/60 = 50$ Hz. As demonstrated in Fig. 13, in the water case, the dominant frequency at the survey points for different tip clearances is concentrated in a low frequency region and at $7f_n$. However, in the gas-liquid two-phase case, the dominant frequency at the survey points is concentrated in a low frequency region, and without the larger pressure fluctuation amplitude at $7f_n$. For the same tip clearance, the amplitude of the pressure fluctuation at the dominant frequency in the gas-liquid two-phase case is at least an order of magnitude smaller than that in the water case. Therefore, in the water case, the pressure fluctuation near the blade tip is mainly due to the strong RSI. However, in the gas-liquid two-phase case, the gas accumulates in the tip clearance, which suppresses the RSI.

To further analyze the variation characteristics of the pressure fluctuation, Fig. 14 demonstrates the

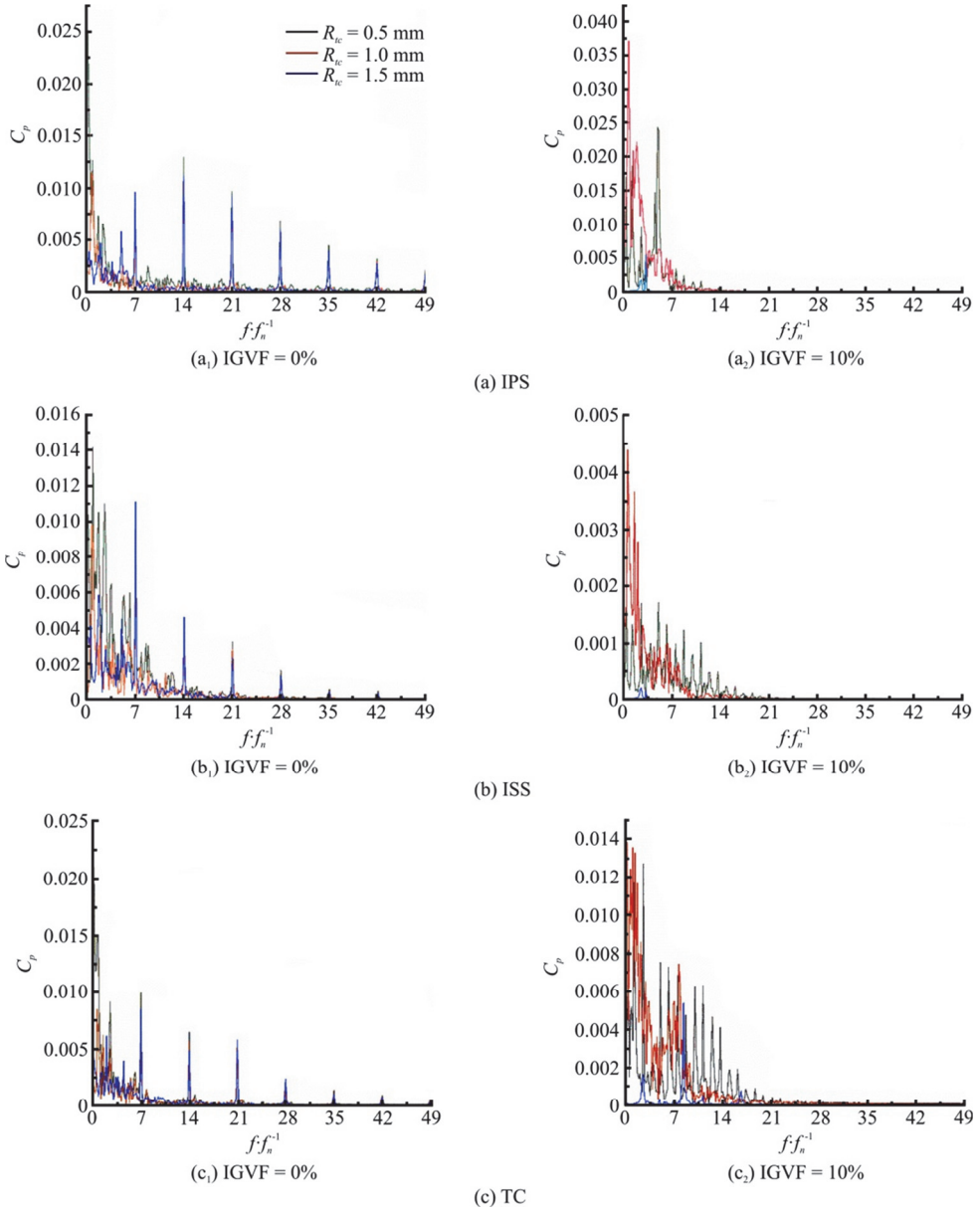

Fig. 13 (Color online) Spectral characteristics near blade tip at the impeller outlet

peak-to-peak values of the pressure fluctuation at the survey points. As presented in Fig. 14, in the gas-liquid two-phase case, the peak-to-peak values of the pressure fluctuation at the survey points are significantly reduced, especially when the tip clearance $R_{tc}=1.5$ mm. In the meantime, the peak-to-peak values at the survey points when the tip clearance $R_{tc}=1.0$ mm are the largest, followed by the peak-to-peak values when the tip clearance $Rt_c=0.5$ mm. Furthermore, in the water case, the peak-to-peak values at the survey points when the tip clearance $R_{tc}=0.5$ mm are larger, as is related to the strong wall jet effect in the small tip clearance.

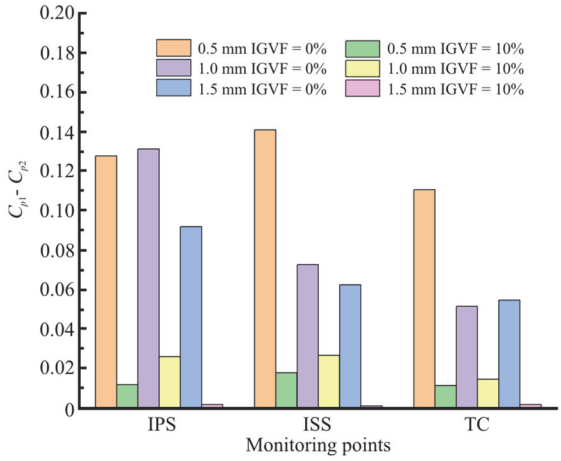

Fig. 14 (Color online) Peak-to-peak values of pressure fluctuation near blade tip at the impeller outlet

Figure 15 illustrates the spectral characteristics of the pressure fluctuation at the survey points near the blade tip at the diffuser inlet for different IGVFs and tip clearances. Figure 15 shows that in the water case, the dominant frequency on the PS and the SS is concentrated at $3f_n$, and the low frequency region and at $3f_n$, respectively. It is demonstrated that the pressure fluctuations in the water case are mainly induced by the RSI. In the gas-liquid case, except in the $R_{tc}=1.5$ mm case, the dominant frequency is concentrated at $3f_n$, and in the other tip clearances, the dominant frequencies are mainly concentrated at the low frequency region. In addition, in the same tip clearance, the amplitude at the dominant frequency is at least one order of magnitude smaller than that in the water case. Meanwhile, the amplitudes in other multiple diffuser BPFs basically disappear in contrast with those in the water case. Thus, the effect of the gas on the pressure fluctuation amplitude at the diffuser blade tip is similar to that at the impeller blade tip.

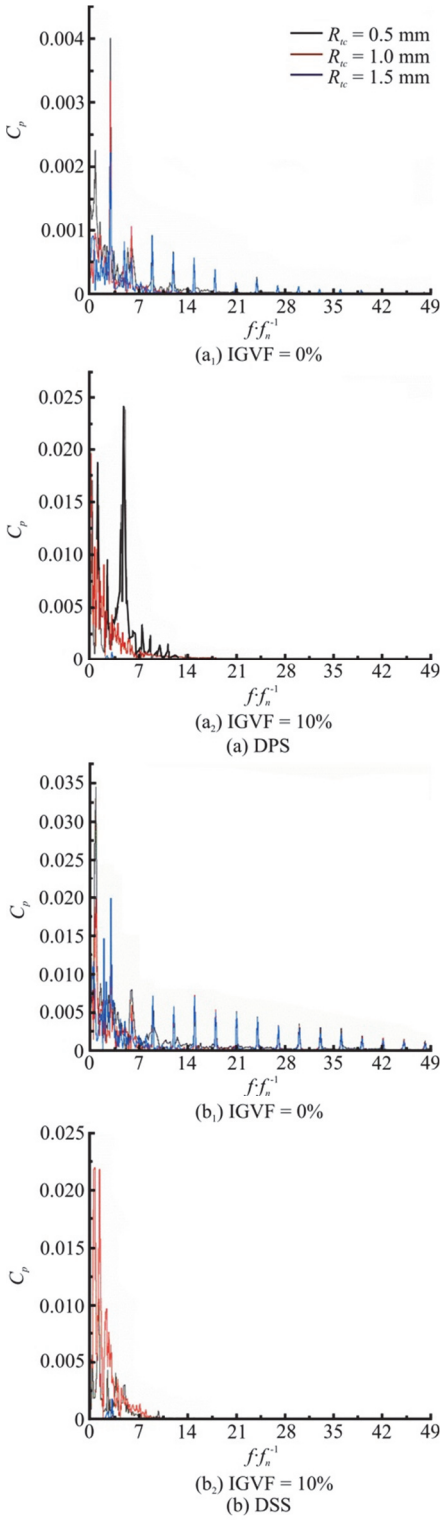

Fig. 15 (Color online) Spectral characteristics of pressure fluctuation near the blade tip at diffuser inlet

Figure 16 displays the peak-to-peak values of the pressure fluctuation at the survey points for different IGVFs and tip clearances. It is shown that in the water case and in the same tip clearance, the peak-to-peak

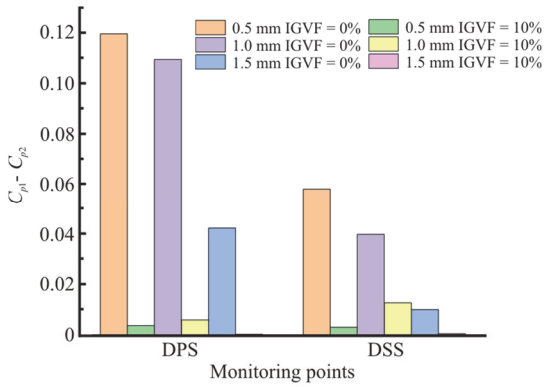

Fig. 16 (Color online) Peak-to-peak values of the pressure fluctuation near the blade tip at diffuser inlet

values of the pressure fluctuation on the PS are larger than those on the SS. In the meantime, the peak-to-peak values of the pressure fluctuation at the survey points in the gas-liquid two-phase case are much smaller than those in the water case. In addition, the maximum peak-to-peak values of the pressure fluctuation on the PS and the SS of the diffuser are both reached when the tip clearance $R_{tc} = 0.5$ mm, as is mainly affected by the TLF from the impeller.

Through the analyses of the pressure fluctuation characteristics near the blade tip of the impeller and the diffuser, the presence of the gas reduces the pressure fluctuation at the BPFs of the impeller and the diffuser, and the amplitude at the dominant frequency is at least an order of magnitude smaller than that in the water case. Meanwhile, the peak-to-peak values of the pressure fluctuation in the gas-liquid two-phase case are smaller than those in the water case.

4. Conclusions

Firstly, the accuracy and the reliability of the numerical simulation are verified with experimental data in the present work. Secondly, the pressure fluctuation characteristics in the multiphase pump are investigated in the water and gas-liquid two-phase cases. Finally, the main conclusions are as follows:

(1) In the water and gas-liquid two-phase cases, the TLV corresponds with the maximum pressure fluctuation intensity. In the meantime, the location of the maximum pressure fluctuation intensity is related to the tip clearance size, and the maximum pressure fluctuation intensity near the blade tip and the hub is the smallest when the tip clearance $R_{tc} = 1.0$ mm. In addition, the pressure fluctuation intensity near the blade tip and the hub at the diffuser outlet decreases with the increase of the tip clearance.

(2) Along the flow direction, the pressure fluctuation trends for different tip clearances in the water and gas-liquid two-phase cases are different, however, in general, the pressure fluctuation intensity is larger near the rotor and stator interface. Furthermore, the pressure fluctuation intensity in the gas-liquid two-phase case is generally larger than that in the water case.

(3) The presence of the gas has a crucial effect on the spectral characteristics of the pressure fluctuation. In the water case, the dominant frequency of the pressure fluctuation at the survey points in the impeller and the diffuser is concentrated at $7f_n$, $3f_n$, respectively. However, in the gas-liquid two-phase case, the dominant frequency of the pressure fluctuation at the survey points is concentrated in the low frequency region. The pressure fluctuations at the multiple impeller and diffuser BPFs gradually disappear, and the dominant frequency amplitude is at least an order of magnitude smaller than that in the water case. Moreover, the peak-to-peak value of the pressure fluctuation in the gas-liquid two-phase case is smaller than that in the water case.

Acknowledgements

This work was supported by the Central Leading Place Scientific and Technological Development Funds for Surface Project (Grant No. 2021ZYD0038), the Open Research Fund Program of State Key Laboratory of Hydroscience and Engineering, Tsinghua University (Grant No. sklhse-2021-E-03) and the Key Scientific Research Fund of Xihua University (Grant No. Z1510417).

References

[1] Kim J., Lee, H., Yoon J. et al. Multi objective optimization of a multiphase pump for offshore plants [C]. *Proceedings of the ASME 2014 4th Joint Us-European Fluids Engineering Division Summer Meeting*, Chicago, IL, USA, 2014.

[2] Hu H., Li X. Gu B. Hydraulic Optimization of multiphase pump based on cfd and genetic algorithm [J]. *International Journal of Grid Distribution Computing*, 2015, 8: 161-170.

[3] Kim J., Lee H., Kim J. et al. Improvement of hydrodynamic performance of a multiphase pump using design of experiment techniques [J]. *Journal of Fluids Engineering*, 2015, 137(8): 081301.

[4] Liu M., Cao S., Cao S. Numerical analysis for interphase forces of gas-liquid flow in a multiphase pump [J]. *Engineering Computations*, 2018, 35(6): 2386-2402.

[5] Zhang W., Yu Z., Zahid M. et al. Study of the gas distribution in a multiphase rotodynamic pump based on interphase force analysis [J]. *Energies*, 2018, 11(5): 1069.

[6] Zhang Y., Zhang J., Zhu H. et al. 3D blade hydraulic design method of the rotodynamic multiphase pump impeller and performance research [J]. *Advances in*

Mechanical Engineering, 2014, 6: 803972.

[7] Shi Y., Zhu H., Yin B. et al. Numerical investigation of two-phase flow characteristics in multiphase pump with split vane impellers [J]. *Journal of Mechanical Science and Technology*, 2019, 33(4): 1651-1661.

[8] Suh J., Kim J., Choi Y. et al. A study on numerical optimization and performance verification of multiphase pump for offshore plant [J]. *Proceedings of the Institution of Mechanical Engineers Part A Journal of Power and Energy*, 2017, 231(5): 382-397.

[9] Suh J., Kim J., Choi Y. et al. Development of numerical Eulerian-Eulerian models for simulating multiphase pumps [J]. *Journal of Petroleum Science and Engineering*, 2018, 162: 588-601.

[10] Zhang J., Tan L. Energy performance and pressure fluctuation of a multiphase pump with different gas volume fractions [J]. *Energies*, 2018, 11(5): 1216.

[11] Zhang D., Shi W., van Esch B. P. M. (Bart) et al. Numerical and experimental investigation of tip leakage vortex trajectory and dynamics in an axial flow pump [J]. *Computers and Fluids*, 2015, 112: 61-71.

[12] Xu Y., Cao S., Sano T. et al. Experimental investigation on transient pressure characteristics in a helico-axial multiphase pump [J]. *Energies*, 2019, 12(3):461.

[13] Shi G., Liu Z., Xiao Y. et al. Effect of the inlet gas void fraction on the tip leakage vortex in a multiphase pump [J]. *Renewable Energy*, 2020, 150: 46-57.

[14] Shi G., Liu Z., Xiao Y. et al. Tip leakage vortex trajectory and dynamics in a multiphase pump at off-design condition [J]. *Renewable Energy*, 2020, 150: 703-711.

[15] Zhang W., Yu Z., Li Y. et al. Numerical analysis of pressure fluctuation in a multiphase rotodynamic pump with air–water two-phase flow [J]. *Oil and Gas Science and Technology*, 2019, 74: 18.

[16] Zhang J., Fan H., Zhang W. et al. Energy performance and flow characteristics of a multiphase pump with different tip clearance sizes [J]. *Advances in Mechanical Engineering*, 2019, 11(1): 1-14.

[17] Feng J., Luo X., Guo P. et al. Influence of tip clearance on pressure fluctuations in an axial flow pump [J]. *Journal of Mechanical Science and Technology*, 2016, 30(4): 1603-1610.

[18] Shen S., Qian Z., Ji B. et al. Numerical investigation of tip flow dynamics and main flow characteristics with varying tip clearance widths for an axial-flow pump [J], *Proceedings of the Institution of Mechanical Engineers*, 2019, 233: 476-488.

[19] Liu Y., Tan L., Hao Y. et al. Energy performance and flow patterns of a mixed-flow pump with different tip clearance sizes [J]. *Energies*, 2017, 10(2): 191.

[20] Hao Y., Tan L., Liu Y. et al. Energy performance and radial force of a mixed-flow pump with symmetrical and unsymmetrical tip clearances [J]. *Energies*, 2017, 10(1): 57.

[21] Zhang W., Yu Z., Zhu B. Numerical study of pressure fluctuation in a gas- liquid two-phase mixed-flow pump [J]. *Energies*, 2017, 10(5): 634.

[22] Wang L., Lu J., Liao W. et al. Numerical simulation of the tip leakage vortex characteristics in a semi-open centrifugal pump [J]. *Applied Sciences*, 2019, 9(23): 5244.

[23] Ayad A., Farid A. M., El-Azm A. Effect of semi-open impeller side clearance on the centrifugal pump performance using CFD [J]. *Aerospace Science and Technology*, 2015, 47: 247-255.

[24] Zheng L., Chen X., Zhang W. et al. Investigation on characteristics of pressure fluctuation in a centrifugal pump with clearance flow [J]. *Journal of Mechanical Science and Technology*, 2020, 34: 3657-3666.

[25] Huan Y. Y., Liu Y. Y., Li X. J. et al. Experimental and numerical investigations of cavitation evolution in a high-speed centrifugal pump with inducer [J]. *Journal of Hydrodynamics*, 2021, 33(1): 140-149.

[26] Han C. Z., Xu S., Cheng H. Y. et al. LES method of the tip clearance vortex cavitation in a propelling pump with special emphasis on the cavitation-vortex interaction [J]. *Journal of Hydrodynamics*, 2020, 32(6): 1212-1216.

[27] Jung J., Joo W. Effect of tip clearance, winglets, and shroud height on the tip leakage in axial flow fans [J]. *International Journal of Refrigeration*, 2018, 93: 195-204.

[28] Syed N., Shafiq R., Malik M. et al. Effect of tip clearance and rotor–stator axial gap on the efficiency of a multistage compressor [J]. *Applied Thermal Engineering*, 2016, 99: 988-995.

[29] Taghavi-Zenouz R., Eslami S. Numerical simulation of unsteady tip clearance flow in an isolated axial compressor rotor blades row [J]. *Proceedings of the Institution of Mechanical Engineers Part C Journal of Mechanical Engineering Science*, 2012, 226(1): 82-93.